



Research article

A key parametric study of ultrasonic exfoliation of 2D TiB₂ using DI water as a unique medium

Marghoob Ahmed^a, Muhammad Aftab Akram^{a,b}, Afsar Bano^c,
Muhammad Zafar Khan^a, Rafia Rehman^d, Rahim Jan^a, Sofia Javed^{a,*}

^a Department of Materials Engineering, School of Chemical & Materials Engineering, National University of Sciences & Technology, Islamabad, 44000, Pakistan

^b Department of Materials Science and Engineering, Pak-Austria Fachhochschule Institute of Applied Sciences and Technology, Mang Haripur, 22620, Khyber Pakhtunkhwa, Pakistan

^c Department of Physics, Syed Babar Ali School of Science and Engineering, Lahore University of Management Sciences, LUMS, 54792, Lahore, Pakistan

^d Section of Phytochemistry and Natural Products, Department of Biological Sciences, National University of Medical Sciences, Rawalpindi, 46000, Punjab, Pakistan

ARTICLE INFO

Keywords:

2D nanomaterials
Transition metal diborides
Ultrasonic exfoliation
Ultrasonic treatment
XRD
SEM

ABSTRACT

Liquid Phase Exfoliation (LPE) is a very effective technique for the synthesis of few layered two dimensional (2D) nanosheets. There is a surge to find environment friendly solvents for efficient exfoliation of layered materials to produce 2D nanosheets. TiB₂ is an important layered material with very little reported work on its 2D nanosheets. The present work is about successful LPE of TiB₂ using deionized (DI) water as a clean, green and low cost dispersion medium to make TiB₂ nanosheets. The impact of ultrasonication conditions i.e. input power and treatment duration for efficient synthesis of few layered 2D nanosheets in DI water is studied by Atomic Force Microscopy (AFM), X-Ray Diffraction (XRD) and Scanning Electron Microscopy (SEM). It is found that by increasing input power, the layer thickness is reduced from bulk to 34 nm with lateral dimensions as huge as up to 5 μm. The increased treatment duration has further reduced the layer thickness to 21 nm associated with a decrease in lateral dimensions to about 1 μm. The mechanism of variation in the aspect ratio of the 2D nanosheets with ultrasonication power and treatment duration is explained. The optimum conditions for the fabrication of high aspect ratio 2D nanosheets of TiB₂ owe to a greater acoustic cavitation intensity, an optimum treatment duration and a homogenous distribution of the cavitation events while using an appropriate size of the sonotrode in the sonicated volume during ultrasonication.

1. Introduction

Two-dimensional (2D) nanomaterials are defined as materials having only one dimension below 100 nm. These nanomaterials (NM) are crystalline, free-standing, sheet-like structures [1]. Precursors of these materials are solids in bulk form with strong covalent or ionic bonds within the layers of atoms and weaker forces holding these layers together. Hence, by applying any shear force or by intercalating agents, these layers can expand in out-of-plane directions or slip in in-plane directions during exfoliation and produce

* Corresponding author.

E-mail address: sofia.javed@scme.nust.edu.pk (S. Javed).

few-layered or monolayered 2D sheets having unique physiochemical properties [2]. These include ultrahigh carrier mobilities, huge surface area, quantum well effects, transparency, increased thermal conductivity, incomparable strength, exceptional optical activities, high flexibility, high stability, and extraordinary carrier transport [3]. 2D nanomaterials find exceptional application in energy storage, sensing, electronics, photodetectors, desalination, minerals recovery, functional inks, drug delivery, and optoelectronic devices [4–7]. The benchmark year for 2D nanomaterials is 2004 when Novoselov and co-workers used micromechanical cleavage method using scotch tape to exfoliate graphite to produce graphene [8].

Transition metal diborides (TMBs) with a stoichiometry MB_2 are ceramics in nature, where M belongs to II-B, IV-B, and V-B groups, e.g., Ti, Zr, Mg, Cr, etc. It is reported that in MB_2 systems, the chemical bonding between boron atoms is covalent [9]. However, the chemical bonding between metal and boron atoms has mixed covalent and ionic bonding [10]. TMBs have a C32 crystal structures with a space group $P6/mmm$. In a hexagonal structure, layers of transition metal atoms are closely packed with alternative graphite like boron atom layers [11]. The existence of various 2D TMBs (also known as MBenes) has been predicted, some of which are made through experimentation [12].

Titanium diboride i.e., (TiB_2) is an important member of borides and has been employed in various high temperature and hard materials applications [13]. A few reports are also found on nanostructured TiB_2 for optoelectronic applications [14]. The crystal structure of TiB_2 has boron atoms placed at 2d (1/3, 2/3, 1/2) “Wyckoff positions”, and transition metal atoms at 1a (0, 0, 0) positions with the $P6/mmm$ (No. 191) space group [15]. The single layer thickness of TiB_2 is roughly around 0.4 nm [16,17]. Although there is some literature on nanostructured TiB_2 but 2D nanosheets of TiB_2 have never been synthesized by LPE using DI water previously. Due to very small single layer thickness, 2D nanosheets of TiB_2 are expected to possess unique properties in comparison to its bulk counterpart.

One of the ongoing challenges in the field of 2D material preparation is achieving a balance between several factors such as quality, cost, scalability, purity, and yield of the 2D sheets [18]. There are several approaches to the synthesis of two-dimensional nanomaterials including bottom-up and top-down routes [19]. The process of using chemical routes or Mechanical Milling enables the large-scale synthesis of the material with a high yield at a relatively low cost. However, the quality of the resulting 2D sheets is compromised because of the presence of defects [20].

Exfoliation is the most popular method used for the fabrication of 2D nanosheets [21]. The conventional method referred to as mechanical exfoliation, has limited feasibility for large-scale industrial use [22]. Liquid phase exfoliation (LPE) has demonstrated significant suitability for large-scale manufacturing and has consequently emerged as the predominant approach for the creation of commercially accessible 2D materials [23–25].

However, the presently employed LPE methods have notable limitations, as outlined in previous studies. These methods typically involve 3 steps that are: (1) the utilization of expensive, hazardous, and environmentally detrimental solvents or surfactants for chemical treatment processing, which aims to increase the interlayer spacing of bulk 2D material; (2) the application of external forces, such as shearing or ultrasonication (US), to facilitate the exfoliation and dispersion of 2D sheets in a solution; and (3) the frequent necessity of purifying 2D sheets to remove any residual chemicals [26–28].

Many solvents like methyl-5-(dimethylamino)-2-methyl-5-oxopentanoate [29], Dimethyl 2-Methylglutarate [30], Cyrene, Polarclean, and Iris [31] have also been reported. All these solvents are expensive and may cause environmental pollution. Therefore, the need to employ environment friendly, non-hazardous dispersants to produce 2D sheets via LPE has been emphasized recently. Hence, De-Ionized (DI) Water is a desirable and attractive choice in this context, particularly due to the hydrophilic properties of many 2D materials [32] and being a cost-effective dispersive medium [33,34]. Several reports on LPE using water as a solvent are found but in the presence of surfactants, polymer stabilizers, or other specialized chemicals as exfoliation agents. These components were deemed essential for achieving the water-dispersed 2D sheets [35,36]. Some studies indicate that a pre-treatment with N-methyl-2-pyrrolidone (NMP), dimethylformamide (DMF), or isopropyl alcohol (IPA) is required before the exfoliation step in water [37,38].

There are very few reports on using altogether benign chemicals for the LPE of TiB_2 . R. Patinder et al. have reported LPE of TiB_2 in IPA and DI water to yield few layered TiB_2 [39]. According to the best of our knowledge, the LPE of TiB_2 using DI water as the only medium has never been reported. Herein, the successful LPE of TiB_2 in DI water as the only dispersion solvent without any additive is being presented along with a mechanistic explanation of the process based on effects of applied ultrasonic power and the treatment duration.

2. Experimental details

2.1. Materials

TiB_2 powder was purchased from PENSOC, China (CAT No. 12045-63-5, 99.9 %), which was used as a BTB for the synthesis of 2D TiB_2 . The particle size was less than 100 μm , as specified by the manufacturer. Deionized water (DIW) was taken from HAT Enterprises, Pakistan, with the purity of Type II to be used as a dispersion medium (DM). NMP, from Merck, Germany (CAS No. 872-50-4, 99.5 %), was used as a DM for the synthesis of 2D TiB_2 for comparison.

2.2. Procedures

Ultrasonication Parameters.

The system (JY91-IIN N&DN Series) used as an Ultrasonic Homogenizer was a probe US transducer with a US horn (sonotrode). As shown schematically in Fig. 1a, the ultrasonic transducer (UST) was used with a 6 mm-diameter titanium alloy sonotrode (ST) with a

piezoceramic transducer working at a maximum frequency of 25 kHz at a maximum power of 650 W (when the sonotrode was used at 100 % input power). The peak-to-peak amplitude of US waves for this setup at a maximum input power of 100 % was 30 μm . A stainless-steel vessel (60 mm diameter) was used to provide good heat dissipation.

The same vessel was used for all the experiments to apply the same geometrically input US waves and to maintain the same volume of DM. The temperature was kept constant at 40 °C by using the water bath. The reason to maintain the system at said temperature is that 2D sheets have better stability at this temperature [40–42]. A standard digital thermometer (DT310LAB) with a stainless-steel probe was used to check the internal system's temperature. The volume or diameter of the cavitation zone (CZ) was 9 mm, as shown in Fig. 1b, which was 1.5 times the diameter of ST [43].

Setup Configuration.

As shown in Fig. 1a and b, the sonotrode was dipped into the liquid 15 mm below the surface and 20 mm above the bottom of the vessel, keeping the ST in the center of the volume of the DM for all the experiments to have the same US configuration.

1 g of BTB and the same volume of DM of 100 ml is used for each setup. The US was applied in the form of pulsed waves with a time interval of 0.2 s on state and 0.1 s off state to have a homogeneous distribution of the energy within the CZ for all the US parameters.

2.2.1. LPE of TiB_2 in DI water

1 g of BTB powder was dissolved in 100 ml of DIW by stirring for 20 min on a magnetic stirring hotplate at room temperature. Then the mixture was transferred to the vessel for the ultrasonic treatment. The LPE was carried out under different conditions varying the ultrasonication power and the treatment duration as mentioned in Table 1. The prepared 2D TiB_2 was separated from bulk and semi-exfoliated TiB_2 by centrifugation at 3000 rpm for 10 min. The supernatant was then dried in a Petri Dish for 24 h at 70 °C in a drying oven (memmert). This made exfoliation in DIW a single-step process in comparison to non aqueous solvents such as N-Methyl pyrrolidone (NMP).

2.2.2. Variation of Ultrasonication Parameters

A Ultrasonication Power

To study the effect of ultrasonic power the LPE OF TiB_2 was carried out at 3 different levels: 390 W (60 %), 520 W (80 %), and 650 W (100 %). The samples were labeled as US-P390 for 390 W, US-P520 for 520 W, and US-P650 for 650 W (Table 1). The energy density of the acoustic waves is given by Equation (1) [44]. Hence, corresponding energy densities (ED) were 84.24 kJ/mL for 390 W, 112.32 kJ/mL for 520 W, and 140.40 kJ/mL for 650 W.

$$\text{Energy Density} = \frac{\text{Power (W)} \times \text{Time (S)}}{\text{Volume (L)}} \quad \text{JL}^{-1} \quad 1$$

B Ultrasonication Duration

In order to get some mechanistic insights into the exfoliation process the effect of the duration of US treatment was studied by conducting the LPE for three different durations: 6 h (labeled as US-T6), 7 h (labeled as US-T7), and 8 h (labeled as US-T8) (Table 1), while maintaining other parameters constant including the input power at 650 W. The ED for 6 h of US was 140.40 kJ/mL, for 7 h it was 163.80 kJ/mL, and for 8 h it was 187.20 kJ/mL.

2.3. Instruments and characterization

All synthesized 2D TiB_2 samples were characterized using the SEM, XRD, and AFM. The details of each characterization technique are given below.

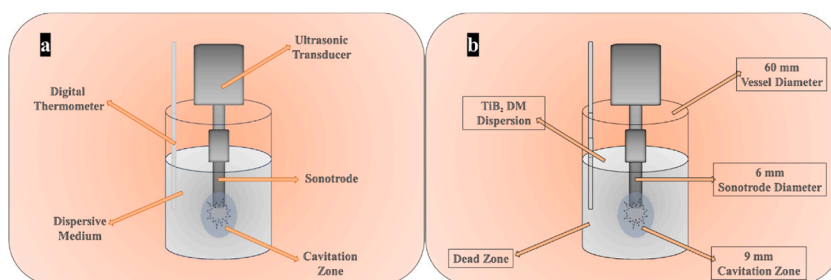


Fig. 1. Schematic representation of Ultrasonic Probe Treatment Setup. 1a: Different parts of the configuration used. 1b: Schematic representation of diameter of sonotrode, vessel, and cavitation zone.

Table 1
The conditions of LPE in DI water for different Experimentaion.

Sr. No.	Sample Code	Treatment Duration (h)	Input Power (W)
1.	US-P390	6	390
2	US-P520	6	520
3	US-P650	6	650
4	US-T6	6	650
5	US-T7	7	650
6	US-T8	8	650

2.3.1. SEM

The lateral dimensions of the sheets were examined by a high-resolution 30-kV scanning electron microscope (SEM) (JEOL-JSM-6490LA). For sample preparation, dispersion was prepared by adding a small amount of 2D TiB₂ i.e., 10 mg, to 15 ml of DIW. The mixture was sonicated in an ultrasonic bath sonicator (WiseClean WUC-A06H) for 1 h at room temperature to have a fine dispersion. For SEM analysis, the samples were drop-cast i.e., 2 to 3 drops of fine dispersion of 2D TiB₂ on a cleaned glass surface. The samples were dried in the drying oven at 60 °C for 3 h. A thin (a few nanometers) conducting gold coating was made on 2D TiB₂ for the conductive surface to get high-resolution imaging. These samples were then analyzed at different magnifications, and the best images with high resolution were taken. Further image processing and lateral dimension measurements were done by ImageJ software. The same process was followed to analyze SEM images of the BTB before the analysis of 2D TiB₂.

2.3.2. AFM

The layer thickness was measured by a very fine probe of the scanning probe microscope (SPM) JSPM-5200 JEOL using atomic forces for the 3D image formation. Atomic force microscopy (AFM) in contact mode with high resolution gives the thickness of the sheets. 5 mg of 2D TiB₂ was added to 15 ml of DIW and placed in a US bath at room temperature for 1 h for dispersion preparation. One drop of the prepared dispersion was drop-cast on a clean, polished Si/SiO₂ surface with negligible roughness. The sample was dried in a vacuum oven for 4 h at 70 °C. The prepared samples were then placed in a vacuum chamber and scanned one by one by AFM.

2.3.3. XRD

For studying the crystal structure and the alignment of sheets of 2D TiB₂ along a specific plane, an X-ray diffractometer (XRD) from Bruker (D2 PHSER diffractometer) was used. For US-BW, US-P390, US-P520, and US-P650, the samples were preheated or dried in the drying oven at 60 °C for 3 h to remove any moisture present or trapped between the layers. Then these dried samples were directly shifted to the stub or sample holder of the XRD for analysis. The same procedure was adopted to study the XRD pattern on BTB. For US-T6, US-T7, and US-T8, 50 mg of 2D TiB₂ was added to 15 ml of DIW and ultrasonicated in the bath sonicator for 1 h at room temperature. Three drops of the prepared suspension were dropped on the cleaned glass substrate. The substrate is then placed in a vacuum oven at 70 °C for 4 h. The dried samples are then placed in sample holders for analysis. All the samples were analyzed from 5° to 80° angle with a slow scan rate.

3. Results and discussion

The LPE of TiB₂ is carried out in DI water as the dispersion medium successfully. The exfoliation parameters are varied to study their effect on the morphology of the resultant 2D nanosheets. The obtained 2D nanosheets are characterized using XRD, SEM and AFM. An explanation of the mechanism involved during the LPE in DI water is also presented. The optimum conditions to fabricate 2D nanosheets with high aspect ratio are deliberated.

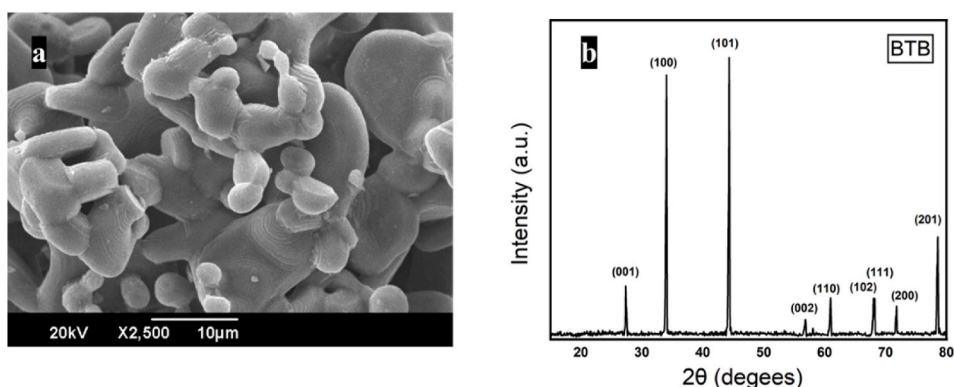


Fig. 2. SEM and XRD image of BTB. 2a: SEM image of BTB showing different morphologies with average particle size between 50 and 100 μm. 2b: XRD plot for BTB.

3.1. Analysis of bulk TiB_2 (BTB)

The XRD and SEM results of BTB are given in Fig. 2a and b. The SEM results indicate that BTB had an average particle size of 50 μm –100 μm (Fig. 2a) The particles show different morphologies with layered structures. TiB_2 is a layered material its different roughness or morphologies help in good exfoliation into 2D nanosheets.

The XRD results have shown that BTB follows a hexagonal crystal structure with a $P6/mmm$ space group. There is a small peak of the (001) plane at the angle of 27.5° , a major peak of the (100) plane at the angle of 34.1° , the most intense peak of the (101) plane at the angle of 44.4° , and a minor peak (200) plane at the angle of 71.904° , as shown by the BTB in Fig. 2b (JCPDS Card No. 01-075-1045).

3.2. 2D TiB_2 nanosheets in DI water

As indicated earlier, there is a surge to find a green DM for the exfoliation of layered materials like TiB_2 . A method to overcome the problems associated with NMP and other solvents is a dire need to improve the resultant 2D nanomaterials. The previous literature indicates the retention of impurities due to solvents like N-Methyl Pyrolidone (NMP) and others, difficulty in scalability as well as requirement of post-treatment and washing as discussed in previous experimental investigations [42].

Herein, successful exfoliation of TiB_2 is carried out for the first time in only DI water. The US cavitation in pure DIW BTB solutions is exclusively employed as a singular procedural step for the exfoliation of 2D TiB_2 . This report provides a manufacturing process for 2D TiB_2 exfoliation in pure DIW carrying the advantages of cleanliness, environmental friendliness, and potential scalability. A similar study has been reported for the large-scale production of graphene by LPE [45]. Notably, this process does not involve the use of any chemical additives or surfactants to yield few layered nanosheets of TiB_2 .

The superiority of the 2D nanosheets obtained by the present method can be analyzed by a comparative study conducted by exfoliating TiB_2 using NMP. The retention of NMP and irregularities in the structure of 2D nanosheets can be observed in the SEM images and XRD plots given in Supporting Information. For the complete removal of NMP, drying at higher temperatures and for a longer duration is required [46]. The impurities can be removed by annealing at elevated temperatures [47]. These processes add more steps, making the process of LPE using NMP as a DM more time-consuming, and complicated. The 2D TiB_2 successfully obtained in DI water is analyzed by studying effects of different process parameters using XRD, SEM and AFM followed by explanation of the mechanism of LPE in DIW.

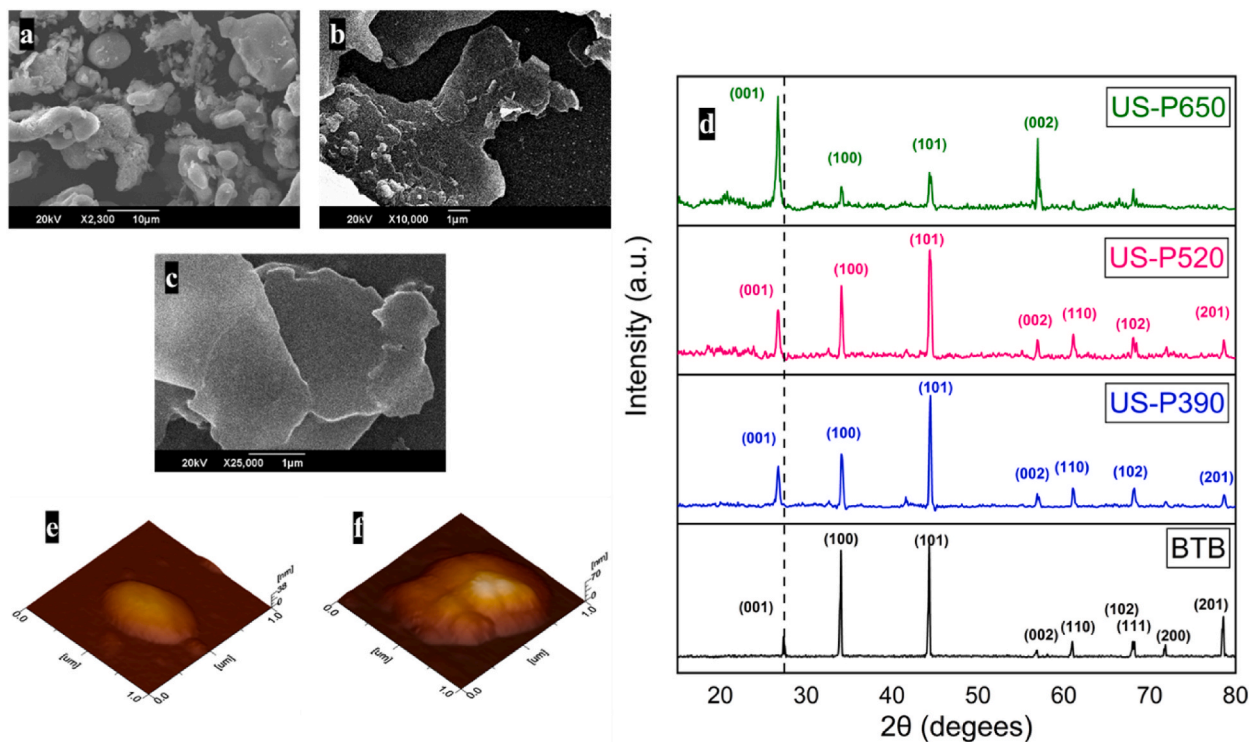


Fig. 3. SEM and XRD images of sample US-P390, US-P520, and US-P650 and AFM images of US-520 and US-650. 3a: SEM image showing the Semi Exfoliated TiB_2 at an input power of 390 W. 3b: SEM image shows a significant amount of layer exfoliation at 520 W input Power. 3c: SEM image shows there is proper exfoliation of sheets of TiB_2 at 650 W input power. 3d: Comparative XRD pattern shows changes in intensities of XRD peaks with peaks shift and peaks broadening. 3e: AFM of the Sample US-P520 showing the layer thickness of around 68 nm. 3f: AFM of sample US-P650 showing that the layer thickness is now reduced to about 35 nm.

3.3. Effect of US parameters

US input power and US duration are the key parameters to control the lateral dimension, layer thickness, and concentration of the 2D dispersion [48]. Hence, the effect of US power and Treatment Time are optimized. The effect of probe size is also studied.

To study the effect of input power, US treatment time is fixed for 6h. While to investigate the effect of the duration (time) of the US treatment, the input power is fixed at 650W, in the light of the power-dependent investigation. All other parameters, setup configurations, and diameter of the sonotrode are fixed, and all the experimentation is performed in DIW as a DM.

3.3.1. Effect of US input power

The first US power utilized was 390 W. The SEM image of sample US-P390 in Fig. 3a shows that the average lateral dimensions are around 10 μm and have a layer thickness of approximately greater than 100 nm. So, there are more than 100 layers in those sheets. The ratio of lateral dimension to layer thickness is found to be around 34. The second US input power was 520 W. The SEM image in Fig. 3b indicates that sample US-P520 has lateral dimensions of around 5 μm –8 μm . There are different sheets with different lateral dimensions, with an average lateral dimension of 6 μm . In the next experiment of the effect of input US power, the value was further increased to 650 W. From the SEM image of sample US-P650 in Fig. 3c, proper 2D sheets can be seen. The lateral dimensions of the sheets are about 5 μm . There is no curling or bending in the sheets.

The XRD results in Fig. 3d for the sample US-P390 (390 W) shows that the intensity of the peak of (001) plane at 2θ 26.9° is increased with a 0.6° shift from the BTB peak. The intensities of the peaks at 34.1° and 44.4° for the planes (100) and (101) is decreased in comparison to that of BTB. There is a slight decrease in the intensities of all other peaks. There is no significant peak broadening nor significant peak shifting of the other planes, which is necessary when we move from bulk to nanoscale regime [40].

For sample US-P520 the peak of the plane (001) is further shifted at 26.8°, and its intensity is increased further due to the perfect

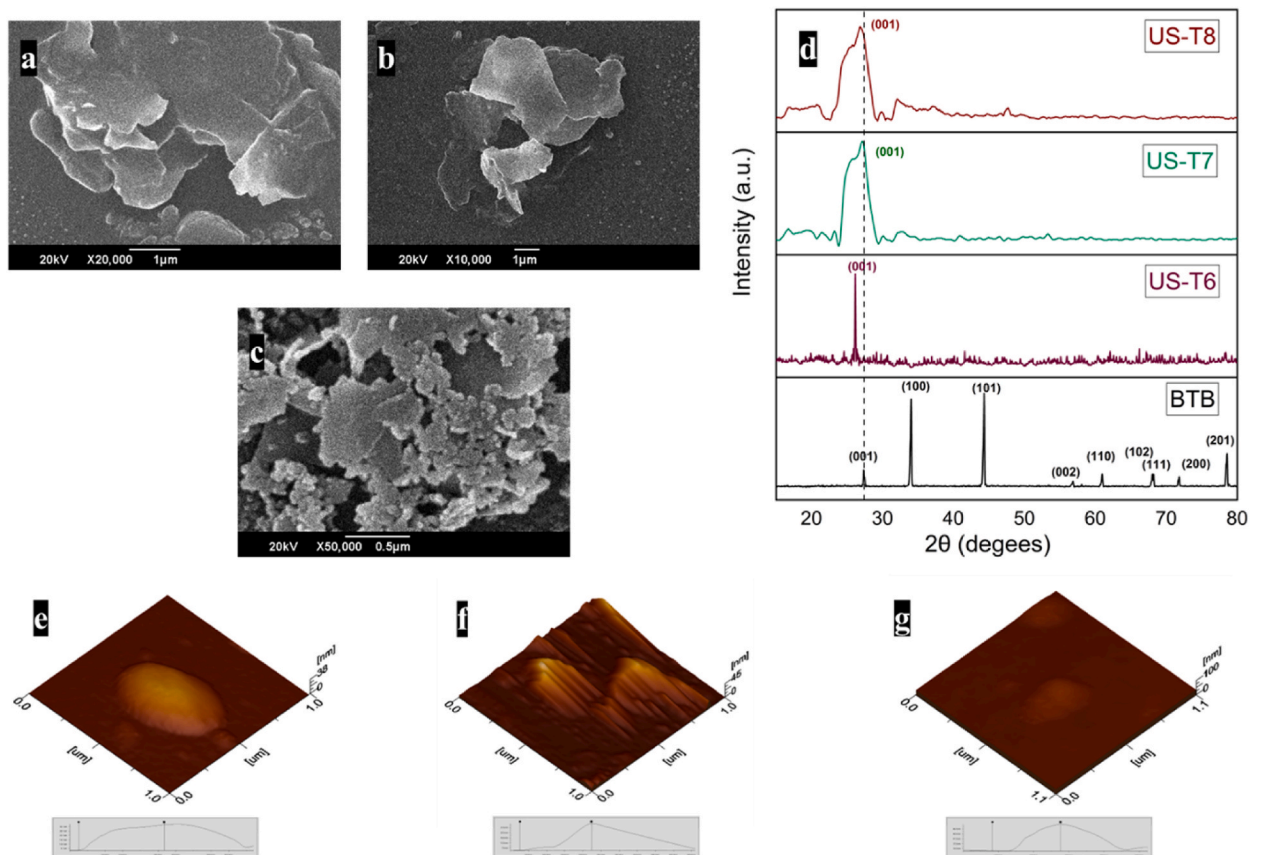


Fig. 4. SEM, XRD, and AFM images of US-T6, US-T7, and US-T8. 4a: SEM image of US-T6 shows the perfect 2D TiB_2 sheets without any defect for 6 h of treatment. 4b: SEM image of US-T7 shows the 2D TiB_2 sheets have no significant defects but there is a breakage lateral dimension for 7 h of US treatment. 4c: SEM image of US-T8 shows that there is significant breakage of lateral dimension 2D TiB_2 with some edge defects 8 h US treatment time 6d: Comparative XRD pattern shows the perfect alignment of sheets along (001) plane with a peak shift and peak broadening which increases with increased duration. 4e: AFM of sample US-T6 showing that the layer thickness was reduced to about 34–35 nm. 4f: AFM of sample US-T7 shows that the layer thickness was reduced to about 31 nm. 4g: AFM of sample US-T8 shows that the layer thickness was now reduced to about 21 nm.. (Line profiles of AFM Images of sample US-T6, US-T7 and US-T8 are also given in SI Separately.)

alignment of the sheets along this plane. The peaks for the planes of (100) and (101) are observed at 34.05° and 44.35° for the sample US-P520, treated at 520W. The intensity of these planes is decreased significantly, which is indicating a reduction in layer thickness as suggested by the early studies. There is also a slight shift in all other peaks, and the intensity of all other peaks is decreased except for the peak of the plane (002) at an angle of 56.85° which support the argument of the alignment of sheets along the (001) plane. There is a peak broadening for all the peaks.

For sample US-P650 the peak intensity of the (001) is further increased, and now it is the highest peak, showing the alignment of most of the sheets along the (001) plane at an angle of 26.6° (with a slight further shift in the peak as compared to the BTB). Now the second most intense peak can be seen to be of the (002) plane at a slightly shifted angle of 56.75° , and the major peaks observed for the BTB i.e. the planes (100) and (101) at angles of 34.0° and 44.3° respectively have negligible intensities. All the other peaks have disappeared due to the alignment of the synthesized nanosheets along a specific direction. All peaks have significant peak broadening, which indicate the presence of 2D TiB_2 with very small thicknesses in nanometers. As evident from the XRD plots, most of the 2D TiB_2 are aligned along the (001) plane. The decrease in the intensity of major peaks indicate that a few layered 2D TiB_2 has been produced.

Further, to see the layer thickness, AFM of US-P520 is done as shown in Fig. 3e. The AFM images show that the layer thickness is around 68 nm which means approximately 140–150 layers of TiB_2 in the sheets are present. The ratio between lateral dimensions and layer thickness is 88, which is greater than that of US-P390. The AFM image of US-P650 in Fig. 3f reveals the layer thickness of about 35 nm. So, there are almost 70 to 80 layers present in the 2D TiB_2 flakes, with the ratio of lateral dimensions to layer thickness of 145.

3.3.2. Effect of US treatment time

Effect of ultrasonic treatment duration is studied by comparing the nanosheets obtained after 6, 7 and 8 h of US treatment. The SEM image of sample US-T6 (6 h) in Fig. 4a shows 2D sheets of TiB_2 with lateral dimensions of around $5 \mu\text{m}$. There is a very narrow distribution of the lateral dimensions of the sheets. Apparently, the sheets are free of structural defects as no curling or bending in the nanosheets is observed. For (Fig. 4b) the sample US-T7, the lateral dimensions are decreased to 2– $4 \mu\text{m}$ with an average of $3.5 \mu\text{m}$. The reduction in the lateral dimension indicates that lateral dimensions have also started to break along with the reduction in layer thickness. These sheets have no significant defects or impurities. The SEM image of 8 h treated sample US-T8 in Fig. 4c shows that the lateral dimensions are further reduced to about $1 \mu\text{m}$. The produced 2D TiB_2 sheets also have some structural defects, and most of the defects were edge related.

In order to conform the alignment of sheets along the specific plane in the US-T6, US-T7 and US-T8, the XRD analysis is carried out after drop casting of dispersion of nanosheets. The XRD plot in Fig. 4d shows that for sample US-6, there is a single intense peak at an angle of 26.1° for the (001) plane with a peak shift of 1.4° . This peak shifting is due to the expansion of the planes within the layers of 2D TiB_2 sheets due to the forces provided by the sonication. There is a peak broadening that shows that the thickness of layers is in the nano range, i.e., sheets are very thin with only a few layers. All other peaks are suppressed for all other planes. All these results confirm that few layered thick 2D nanosheets of TiB_2 that are perfectly aligned with the (001) plane are obtained.

From the XRD pattern of the sample US-T7, an intense broad peak for the (001) planes can be seen (Fig. 4 d). The angle of this peak is 25.9° (with a shift of 1.6° as compared to the peak of BTB). The peak broadening shows that the layer thickness is in the nano range, i.e., sheets are a few layers thick. The shift in the angle are due to the expansion of the planes due to the shear forces for ultrasonic cavitation. The asymmetry of the peak is for the reason that there are sheets of different lateral dimensions with a relatively larger distribution. So, the sheets with smaller lateral dimensions have less effect on d spacing as compared to the sheets with larger lateral dimensions, so they show a little more shift, producing a single broad asymmetric peak.

The XRD pattern of the sample US-T8 has a very broad, intense peak of the plane (001) with a small shift of 2.0° as compared to the peak of BTB at an angle of 25.5° . This shift in the peak shows further reduction of the layered thickness as the effect of the shear forces on the planes increase; hence, there is a little more expansion of the planes within the sheets. The significant peak broadening suggest

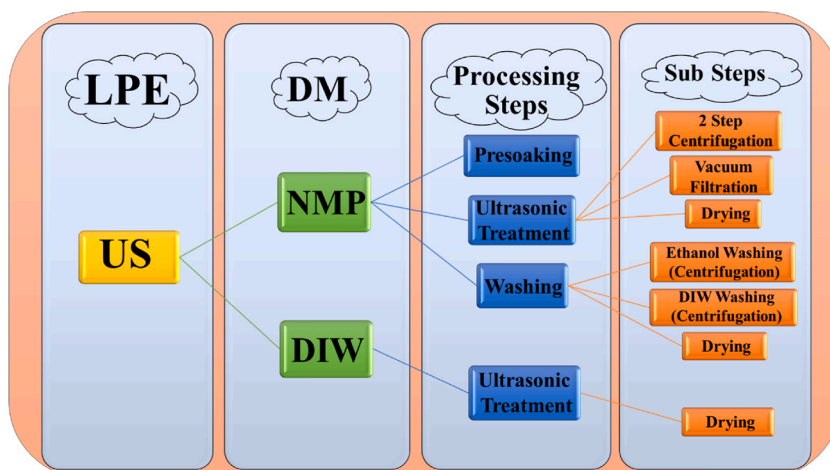


Fig. 5. The comparative flow chart of the LPE processes by US treatment using NMP and DIW as DM.

that as the treatment duration is increased to 8 h, the lateral dimensions also start to break. The peak is asymmetric due he the reason mentioned above.

The AFM is carried out to measure the thickness of 2D flakes obtained after different treatment durations. It is observed that the average flake thickness is found to be around 34 nm (i.e. 68 to 77 layers) with the ratio of the lateral dimension to the layer thickness of around 148 for sample US-T6 (Fig. 4e). With an increase in the treatment duration to 7 h (US-T7) the average layer thickness is reduced to about 31 nm with 60–65 sheets in the 2D flakes. There is also a reduction in the ratio of lateral dimension to layer thickness to 110 (Fig. 4f). Further increase in the US treatment duration to 8 h (US-T8 Fig. 4g), leads to further reduction in the thickness of the 2D nanosheets to about 21 nm with approximately 40–44 atomic layers of TiB_2) With a significant reduction in the lateral dimensions to layer thickness ratio to 47. The reduction in the lateral dimensions are also evident from the SEM images.

3.4. Significance of DIW over non aqueous solvents

As mentioned earlier, the synthesis of 2D sheets using non aqueous solvent is usually a three step process which required the removal of solvent from sheets at the end of process. So for comparative study, LPE is carried out in NMP (see SI). Fig. 5 summarizes the advantages of using DIW over NMP as a flow chart of the LPE process. It can be seen from the figure that the LPE process in NMP as DM was a three-step process. There are many sub-steps in these three major steps, making this process lengthy, much more time-consuming, and laborious. On the other hand, the LPE process in DIW as DM was a single-step process. This one-step process had only a few sub-steps, which made this LPE a fast, easy, and cheap process.

Moreover, the 2D TiB_2 nanosheets synthesized in DIW have no impurities or defects. Also, 2D nanosheets prepared in DIW have larger lateral dimensions as compared to those prepared in NMP(see SI). Table 2 shows the comparison of the properties of 2D TiB_2 sheets prepared in NMP and DIW.

3.5. Significance of US parameters

From the XRD, SEM and AFM results of TiB_2 nanosheets obtained at different input powers indicate that upon increasing the input power the number of layers in the 2D nanosheets flake decreases as well as the aspect ratio increases (Table 2) The comparison of the produced sheets at different input powers shown by the XRD pattern in Fig. 5d reveals that by increasing power, the intensities of different peaks change along with an increase in peak shift and broadening. The alignment of sheets along the (001) plane also increases. The graph in Fig. 6a shows that the energy density and hence, the Inertial Cavitation Dosage (ICD) are directly proportional to the input power. By increasing the input power, the ED supplied to the DM for the exfoliation of 2D TiB_2 can be increased in the CZ of US.

By increasing the energy density from 84.24 kJ/mL (at 390 W) to 112.32 kJ/mL (at 520 W) and then finally to 140.40 kJ/mL (650 W), the ICD is increased, and hence the cavitation field's (CF) strength is increased. At 140.40 kJ/mL of energy density, the ICD is so strong that it provides a handsome amount of force to the layers of BTB and exfoliates them into a 2D TiB_2 . The lateral dimensions show a decrease from 10 μm to 5 μm . The layer thickness decreases significantly from greater than 100 to 35 nm. The ratio of lateral dimensions to layer thickness increases significantly from 34 to 145. This shows that by increasing power, layer thickness decreases, and the degree of exfoliation increases with an increased concentration of 2D TiB_2 dispersion as shown in Fig. 7. The effect of power on the nanosheets is shown in Table 3.

The effect of change in the duration of US treatment can be explained using the SEM, XRD and AFM results shown in Fig. 3. The XRD patterns show a significant peak shift and change in the intensities that conformed to the production of 2D nanosheets of TiB_2 for all durations, with a high degree of exfoliation and perfect alignment along the (001) plane. But peak broadening is enhanced with increased US treatment duration, which displays the breakage of lateral dimensions along with layer thickness. This effect intensifies with increased duration. The variation of US treatment time with a fixed input power results in large sheets of perfectly exfoliated TiB_2 nanosheets and high lateral dimension to thickness ratio for 6 h treatment.

The graph in Fig. 6b shows that the US duration also has the same effect on the ED supplied to the system by the UST, and hence the ICD varies directly with the time of the ultrasonication. By increasing the ED from 140.4 kJ/mL(6h UST) to 163.8 kJ/mL(7h UST) and then finally to 187.2 kJ/mL (8h UST), the effect of ICD is increased, and hence the CF strength provided for a longer time. At 187.2 kJ/mL of energy density, the ICD becomes so strong that it provides a handsome amount of force for a longer time to the layers of BTB, which not only exfoliates them into 2D TiB_2 but also breaks the nanosheets (reducing the lateral dimensions) as shown in Fig. 7. By increasing UST time from 6-h to 8-h, the layer thickness is reduced from 34 to 21 nm. While the lateral dimensions decrease significantly from 5 μm to 1 μm , significantly reducing the ratio of lateral dimensions to layer thickness from 148 to 47. Defects are also introduced to some extent for a longer time. The effect of US treatment duration on the produced nanosheets is shown in Table 4.

Table 2

The comparison of the different properties of produced sheets in two different DMs, i.e., NMP and DIW.

Process	Impurities	Lateral dimensions	Structural Defects	Processing Time
NMP	Present	Smaller	Can be present	Long
DIW	Not present	Larger	No defects	Less

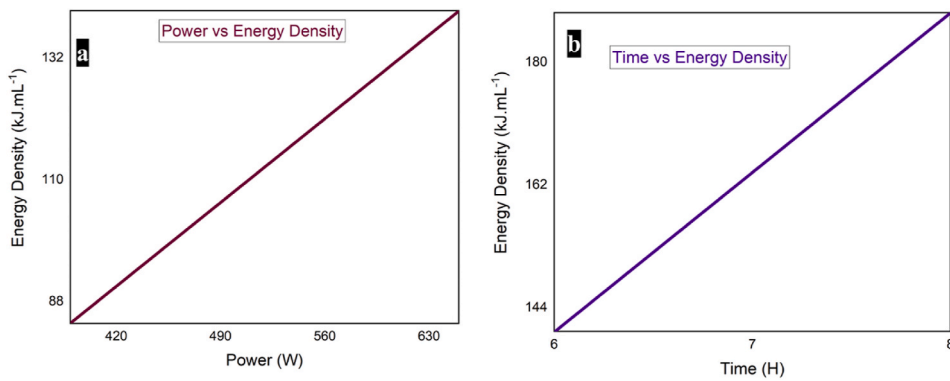


Fig. 6. Variation of Energy density provided to dispersive medium in cavitation zone by ICD as a Function of Input Power and US treatment time. 6a: Graph between Energy density and input power shows. 6b: Variation of Energy density as a Function of time.

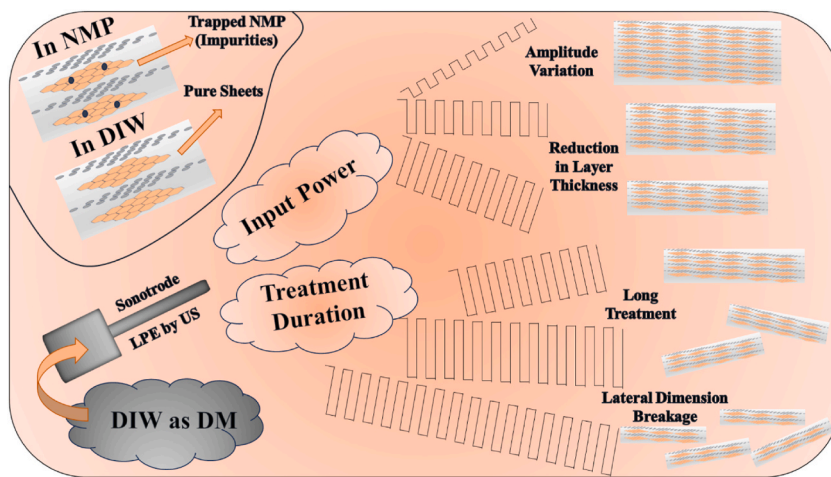


Fig. 7. Schematic representation of the effect of LPE by US in different solvents and the influence of different ultrasonic parameters.

Table 3

The effect of change in input power on the properties of produced 2D TiB₂ showing the enhancement of exfoliation with increased power.

Input Power (W)	Energy Density (kJ/mL)	Lateral Dimensions (μm)	Layer Thickness (nm)	The ratio of Lateral dimensions to layer thickness	Structural Defects	Impurities	Treatment Duration (h)
390 (US-390)	84.24	10	>100	34	No	No	6
520 (US-520)	112.32	6	68	88	No	No	
650 (US-650)	140.40	5	35	145	No	No	

Table 4

The effect of the change of US treatment duration on the properties of produced 2D TiB₂ shows the significant breakage of lateral dimension with increased duration.

Treatment Duration (h)	Energy Density (kJ/mL)	Lateral Dimensions (μm)	Layer Thickness (nm)	The ratio of Lateral dimensions to layer thickness	Structural Defects	Impurities	Input Power (W)
6 (US-T6)	140.40	5	34	148	No	No	650
7 (US-T7)	163.80	3.5	31	110	Not Significant	No	
8 (US-T8)	187.20	<1	21	47	Up to some extent	No	

3.6. Mechanism of US exfoliation using DIW

The formation of cavitation in LPE is contingent upon the acoustic power (AP), whereas the intensity of cavitation (CI) is directly proportional to the energy generated by the bubbles. The relationship (shown in equation (2)) between the driving frequency (f) and squared vibration amplitude (A^2) (which depends upon the input power) is responsible for determining the acoustic power (W), which in turn influences the average bubble size. Similarly, the acoustic power (W) affects the concentration of bubbles. Here, ρ is the DM (DIW) density, c is the velocity of US waves in the DM [45,49].

$$\text{Cavitation Intensity (input power of acoustic field)} = 2\pi\rho c \times f^2 A^2 \times \frac{\pi\phi^2}{4} \quad 2$$

The input power results showed that initially, the AP was not enough to exfoliate the layers of 2D TiB₂. The CI in the CZ was very weak. Hence, there were fewer bubbles produced by the US with larger sizes [50]. The pressure generated by the cavitation and its distribution within the volume of the CZ were not enough to produce an effective exfoliation by the cavitation produced by these bubbles [51]. That is why the exfoliation rate (degree of exfoliation) was low because of the combined effect of the size, activity, and concentration of the cavitation bubbles [52]. Hence, at low AP, there were large sheets of semi-exfoliated TiB₂. These sheets were of larger sizes and had many layers of material. By increasing the AP, the cavitation field's strength was increased. At higher AP, the CF was so strong that it provided a handsome amount of force to the layers of BTB and exfoliated them into 2D TiB₂ [33]. Hence, this shows that by increasing power, layer thickness decreases, and the degree of exfoliation increases with increased concentration.

The inertial cavitation dosage (ICD) is determined by the energy density (ED) of the bubbles, which depends on the treatment time (t) and the input power (W), which are the major factors in controlling the amount of energy delivered to the BTB layers. The formula for calculating ED is given in Equation (1) [44]. The ratio between the CZ volume (v) and the treated volume, or volume of the liquid (V), is given in Equation (3) [52]. This ratio defined the distribution of the energy of US cavitation with the volume of the vessel [45].

$$\text{Energy Density} = \frac{\text{Power (W)} \times \text{Time (S)}}{\text{Volume (L)}} \quad JL^{-1}$$

$$\frac{v_{6mm}}{V} = 0.0034 \quad 3$$

Thus, for less treatment time, the cavitation intensity was good enough, and the size, concentration, and activity of the bubbles were so high that they produced considerable pressure within the CZ [53]. The distribution of the pressure and energy density was in such a way that shear forces mostly acted to separate the layers without breaking them. The CF provided a sufficient ICD within the cavitation zone. With the prolonged US treatment, the pressure produced by the bubbles was applied for a longer time, and smaller bubbles with larger numbers were produced for a longer time. The cavitation field intensity acted in such a way that it started to break the sheets as well, along with their exfoliation [54,55].

To comprehend the significance of US configuration geometry in the context of this study, let's compare the XRD plots in Fig. 6d of the samples US-T6, US-T7, and US-T8. There was a significant peak broadening with increased treatment time, indicating the breakage of the lateral dimensions. The SEM results in Fig. 4a, b, and 4c also show the same results. The main reason for the breakage of the sheets was the diameter or size of the sonotrode. While operating at the same frequency of around 25 kHz and power of 650 W (maintaining the same amplitude), a consistent cavitation intensity was provided. However, by increasing treatment time, the effect of the cavitation field or intensity was increased, which increased the energy density and hence the ICD provided to the dispersive medium by the sonotrode [54,55]. For a 6-mm ST, the US field exhibited a greater degree of heterogeneity. This was characterized by the release of acoustic energy close to the sonotrode tip, resulting in the formation of a highly concentrated CZ [45]. This CZ expanded downward in a conical structure and experienced rapid attenuation due to the shielding effect [52]. Consequently, there were regions within the vessel that were further away from the tip, which were "dead zones" [45]. This effect remains almost the same even if we consider the secondary acoustic fluxes, as they are negligible in the case of smaller diameter ST [56]. Hence, the 6-mm ST resulted in a concentrated CZ. The CZ was about 1.5 times the diameter of the ST [43]. This suggested that there was a difference of 9 mm and 60 mm in the diameter of the active CZ and the size of the vessel, as seen in Fig. 1b. Hence, it can be shown that the 6-mm ST effectively produced a cavitation region that covered only a portion of the treated volume, and the region away from the ST tip was in the "dead zone". Due to this heterogeneous distribution of the CF, the ED acted on the sheets in such a way that it broke the lateral dimension considerably along with the reduction of layer thickness. This effect was enhanced by the long treatment time.

If the sonotrode tip with a greater diameter is used, the distribution of the US field throughout the solution volume will become increasingly uniform, especially when the diameters of ST and vessel approach closer proximity to each other, providing a homogenous CZ. The homogeneous cavitation treatment will yield a more consistent distribution of a few layers of 2D TiB₂ (FLTb) sheets in terms of size and thickness. This contrasts with the configuration with a concentrated CZ. Hence, the smaller ST, while having the same input power, exhibited a greater concentration of cavitation in a smaller volume. Consequently, this led to an increased number of chances for the production of faulty structures in the final sheets of 2D TiB₂ [45].

The mechanisms behind the process of Sonoexfoliation (US LPE) of 2D TiB₂ sheets are intricately linked to the well-established regime of cavitation. The primary mechanism behind LPE through cavitation, like other solvent processes in the US, involves the collapse of microscale bubbles that are undergoing intense oscillations [50]. The characteristics of bubbles, i.e., size, distribution, quantity, collapse, and spatial distribution of these bubbles in the vessel, are significant factors that are influenced by the frequency, power (amplitude), treatment time, and configuration geometry of the set-up [57]. The schematic representation of the LPE of 2D TiB₂

by the US is shown in Fig. 8.

The Minnaert equation provides a prediction about the linear resonance size (LRS) of bubbles [58,59]. This LRS, at which the bubble undergoes instability and collapses, is influenced by the acoustic frequency and power. In the case of water at around 25 kHz and 100 % power, the predicted LRS of the bubble was approximately 140 μm [60]. The bubbles possess a significant amount of potential energy. The bubbles within that specific range of resonance size have a propensity to collapse when subjected to appropriate LRS. Upon experiencing a catastrophic collapse, the energy is promptly discharged, resulting in the formation of liquid micro-jets (LMJ) at the nanoscale [61] with high velocities ranging from 100 to 500 m/s [62]. The previous experimental results show that the LMJ tip is around one-tenth of the maximum or resonant bubble radius of [62]. The size and duration of cavitation bubbles can vary, and they can exhibit both individual and collective behavior, i.e., as a cloud of bubbles [52]. This collective behavior can have a substantial impact on the dynamics of bubbles. Additionally, the behavior of cavitation bubbles can be either steady or transitory, depending on the characteristics of the acoustic pressure field they are subjected to Ref. [51]. These events play a crucial role in governing the cavitation process and potentially influencing the mechanism of BTB exfoliation. Given the inherent chaos and dynamism of the environment, it is not feasible to exert direct control over the individual behavior of bubbles. Consequently, adjustments to the US parameters are made by observing the collective behavior of bubble clouds and the resultant pressure waves. This monitoring process informs the necessary modifications to the US parameters [45]. Furthermore, because of the chain reactions and multiplication of cavitation bubbles (CB) [49,63], the initial collapse is accompanied by the generation of smaller bubbles of reduced dimensions, commonly referred to as nanobubbles [64]. The nanobubbles generated in the chain reaction exhibit a size exceeding 30 nm [64], which is larger than the interlayer spacing of TiB_2 . However, they remain susceptible to excitation from shock waves or the incident frequency of 25 kHz, leading to vigorous oscillations and the generation of various vibrating modes known as "Faraday or surface waves" (SW) [65]. The resonance of SW with a frequency in the MHz range gives rise to the formation of unstable, highly non-linear, chaotic, and dynamic structures [66]. The bubble pressures have the potential to reach many hundreds of kilopascals (kPa) [65,66]. The produced high-pressure shock waves reach up to 1 GPa [67,68], and localized regions of elevated temperature up to 10^4 K are produced [69,70]. This process is iterated several times within a single second which is sufficient to cause the exfoliation of the layers in TiB_2 , and is widely regarded as the primary mechanism behind the exfoliation of 2D materials as shown in the studies [71].

Based on the information provided, it can be inferred that the high-frequency or high-power US treatment with an ST diameter comparable to the diameter of the vessel exhibited a comparatively gentle emission of jets, likely attributable to the forceful contraction or implosion action. Such treatment was deemed more appropriate for exfoliating purposes as it resulted in the formation of CB of smaller sizes. As the frequency increased, the size of the collapsing CB and the period of the collapse decreased by Ref. [72]. In contrast, the utilization of an ST operating at a lower frequency or power results in the formation of bigger CBs that exhibit more forceful collapse. This phenomenon potentially enhances the dispersion of sheets, thereby yielding a greater concentration of FLTB sheets in the solution. However, it is important to note that this approach also generates a substantial quantity of smaller cavitation bubbles. Micrometer-sized CB has the potential to fracture the lateral dimensions of sheets in a direction that is perpendicular to the TiB_2 planes. Conversely, smaller bubbles are believed to delicately extend the interlayer spacing inside the TiB_2 layers [45].

The potential for industrial scale-up appears promising when considering the combination of the two techniques i.e., US bath sonicator (BUS) and US Probe Sonicator (PUS) for inducing cavitation. This aligns with findings reported in other studies, where the authors utilized a combination of a BUS of 30 kHz and a PUS sonotrode of 20 kHz, together with surfactants and chemical exfoliation agents [33]. Sonochemistry offers an additional mechanism for cavitation-induced exfoliation in aqueous environments. The process of layer-by-layer 2D sheet exfoliation in DIW is attributed mainly to a sonochemical reaction of the free radicals generated by the collapse of CB, as stated in a previous study [40]. The US process was conducted at two distinct temperatures, specifically 40 °C and 60 °C, within a 40-kHz BUS for 60 h. The researchers concluded that the observed exfoliation phenomenon was only attributed to the

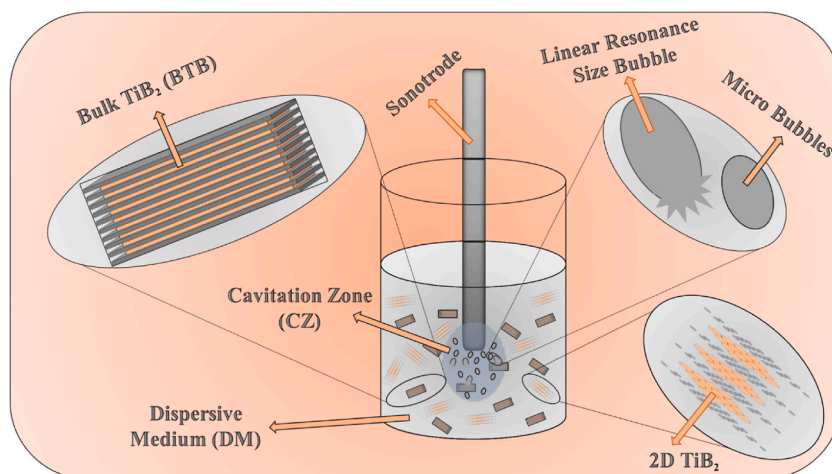


Fig. 8. Schematic representation of the US processing by LPE of 2D TiB_2 . Sheets of 2D TiB_2 have layers of Titanium atoms sandwiched between the hexagonal arrangements of the Boron atoms.

occurrence of cavitation, which was exclusively achieved at the higher temperature (60 °C). This study only focuses on the field of chemistry, with little attention given to the comprehensive investigation of US characteristics and cavitation.

From this study, it can be concluded that 2D TiB₂ nanosheets exfoliation during US cavitation treatment involves physico-mechanical processes. The process of exfoliation studied by high-speed photography techniques can show that TiB₂ sheet splitting occurs because of oscillating and collapsing CB as shown in a previous study [71]. This research provided a good illustration of the process by which CB, originating from the ST tip, causes the fragmentation of 2D nanosheets. Subsequently, these CBs progressively exfoliate the sheets by penetrating the interlayer spaces inside the bulk-layered structure [71].

Further research can be done by utilizing in-situ observations for the examination of cavitation-induced exfoliation by multiple ultrasonic sources with varying frequency ranges, power levels, geometrical configurations, sonotrode sizes and configurations, treatment durations, and setups to produce larger 2D TiB₂ sheets with consistent lateral dimensions, thickness, and a significantly high yield suitable for industrial or practical large-scale manufacturing purposes. Further investigation is required to explore the potential application of two-dimensional titanium diboride (2D TiB₂).

4. Conclusions

It can be concluded that highly pure, defect free 2D nanosheets of TiB₂ are produced by Liquid Phase Exfoliation in the present study. DI water (in the absence of any chemical surfactants or additives) has proved to be an efficient DM for this purpose. The effects of various US LPE parameters, specifically the input power and treatment time on the characteristics of produced 2D TiB₂ nanosheets are also studied. The utilization of different powers shows a decrease in the mean thickness of the resulting 2D sheets. The increased treatment time breaks down the lateral dimensions too. The most optimal outcomes with large lateral dimensions (about 5 μm) and reduced thickness of around 35 nm are achieved using a sonotrode operating at 650 W input power for 6 h treatment time. The LPE process for the exfoliation of 2D TiB₂ in water is attributed to the mechanical effects of tiny active cavitation bubbles, which facilitate the dispersion and exfoliation to a few layered 2D TiB₂ nanosheets. Also, the exfoliation in DIW is much cheaper, can easily be scaled up and requires very little time being a single-step process. The produced high-quality, pure nanosheets of 2D TiB₂ can be used in energy storage, water splitting, or photocatalytic applications.

Data availability statement

Data will be made available on request.

CRediT authorship contribution statement

Marghoob Ahmed: Writing – review & editing, Writing – original draft, Visualization, Validation, Methodology, Investigation, Formal analysis, Data curation, Conceptualization. **Muhammad Aftab Akram:** Writing – review & editing, Formal analysis. **Afsar Bano:** Writing – review & editing, Methodology, Formal analysis, Data curation, Conceptualization. **Muhammad Zafar Khan:** Writing – review & editing, Data curation. **Rafia Rehman:** Writing – review & editing, Formal analysis, Conceptualization. **Rahim Jan:** Writing – review & editing, Resources. **Sofia Javed:** Writing – review & editing, Supervision, Resources, Conceptualization.

Declaration of competing interest

The authors declare that they have no known competing financial interests or personal relationships that could have appeared to influence the work reported in this paper.

Supporting Information

SEM and XRD results of samples prepared in NMP before and after the washing process of the procedure sheets are given in supporting information. **Line profiles** of the AFM images of samples US-T6, US-T7, and US-T8.

Appendix A. Supplementary data

Supplementary data to this article can be found online at <https://doi.org/10.1016/j.heliyon.2024.e29417>.

References

- [1] N. Baig, Two-dimensional nanomaterials: a critical review of recent progress, properties, applications, and future directions, *Compos. Appl. Sci. Manuf.* (2022) 107362.
- [2] M.S. Stark, et al., Intercalation of layered materials from bulk to 2D, *Adv. Mater.* 31 (27) (2019) 1808213.
- [3] A. Gupta, T. Sakhivel, S. Seal, Recent development in 2D materials beyond graphene, *Prog. Mater. Sci.* 73 (2015) 44–126.
- [4] Y. Wang, et al., Two-dimensional nanomaterials with engineered bandgap: synthesis, properties, applications, *Nano Today* 37 (2021) 101059.

- [5] M. Frappa, et al., A few-layer graphene for advanced composite PVDF membranes dedicated to water desalination: a comparative study, *Nanoscale Adv.* 2 (10) (2020) 4728–4739.
- [6] A. Gugliuzza, et al., Prospects of 2D materials-based membranes in water desalination, *Chem. Eng. Trans* 73 (2019).
- [7] S. Santoro, et al., Lithium recovery through WS₂ nanofillers-promoted solar photothermal membrane crystallization of LiCl, *Desalination* 546 (2023) 116186.
- [8] K.S. Novoselov, et al., Electric field effect in atomically thin carbon films, *Science* 306 (5696) (2004) 666–669.
- [9] P. Vajeeston, et al., Electronic structure, bonding, and ground-state properties of AlB₂-type transition-metal diborides, *Phys. Rev. B* 63 (4) (2001) 045115.
- [10] F.R. Wagner, et al., A position-space view on chemical bonding in metal diborides with AlB₂ type of crystal structure, *Z. Anorg. Allg. Chem.* 639 (11) (2013) 2025–2035.
- [11] H. Ihara, M. Hirabayashi, H. Nakagawa, Band structure and x-ray photoelectron spectrum of Zr B₂, *Phys. Rev. B* 16 (2) (1977) 726.
- [12] V.G. Nair, et al., 2D MBenes: a novel member in the flatland, *Adv. Mater.* 34 (23) (2022) 2108840.
- [13] A. Saurabh, et al., Titanium-based materials: synthesis, properties, and applications, *Mater. Today: Proc.* 56 (2022) 412–419.
- [14] A. Sharma, A. Thakur, V. Rangra, Excitonic effects on the optical spectra of TiB₂ nanosheets, *J. Phys. Condens. Matter* 36 (4) (2023) 045501.
- [15] B. Mouffok, H. Feraoun, H. Aourag, Electronic structure of some mono-, semi-titanium boride and diboride, *Mater. Lett.* 60 (12) (2006) 1433–1436.
- [16] I.R. Shein, A.L. Ivanovskii, Elastic properties of mono- and polycrystalline hexagonal AlB₂-like diborides of s, p and d metals from first-principles calculations, *J. Phys. Condens. Matter* 20 (41) (2008) 415218.
- [17] M.Q. Zhao, et al., Scalable manufacturing of large and flexible sheets of MXene/graphene heterostructures, *Advanced Materials Technologies* 4 (5) (2019) 1800639.
- [18] R. Raccichini, et al., The role of graphene for electrochemical energy storage, *Nat. Mater.* 14 (3) (2015) 271–279.
- [19] A. Yadav, et al., Synthesis, processing, and applications of 2D (nano) materials: a sustainable approach, *Surface. Interfac.* 39 (2023) 102925.
- [20] S.H. Choi, et al., Large-scale synthesis of graphene and other 2D materials towards industrialization, *Nat. Commun.* 13 (1) (2022) 1484.
- [21] L. Niu, et al., Production of two-dimensional nanomaterials via liquid-based direct exfoliation, *Small* 12 (3) (2016) 272–293.
- [22] E. Gao, et al., Mechanical exfoliation of two-dimensional materials, *J. Mech. Phys. Solid.* 115 (2018) 248–262.
- [23] K.R. Paton, et al., Scalable production of large quantities of defect-free few-layer graphene by shear exfoliation in liquids, *Nat. Mater.* 13 (6) (2014) 624–630.
- [24] M. Cai, et al., Methods of graphite exfoliation, *J. Mater. Chem.* 22 (48) (2012) 24992–25002.
- [25] J.M. Tour, Scaling up exfoliation, *Nat. Mater.* 13 (6) (2014) 545–546.
- [26] Y. Jiang, et al., Simulating powder X-ray diffraction patterns of two-dimensional materials, *Inorg. Chem.* 57 (24) (2018) 15123–15132.
- [27] A. Ciesielski, P. Samorì, Graphene via sonication assisted liquid-phase exfoliation, *Chem. Soc. Rev.* 43 (1) (2014) 381–398.
- [28] M. Lotya, et al., High-concentration, surfactant-stabilized graphene dispersions, *ACS Nano* 4 (6) (2010) 3155–3162.
- [29] V. Paolucci, et al., Sustainable liquid-phase exfoliation of layered materials with nontoxic polarclean solvent, *ACS Sustain. Chem. Eng.* 8 (51) (2020) 18830–18840.
- [30] G. D'Olimpio, et al., Dimethyl 2-methylglutarate (Iris): a green platform for efficient liquid-phase exfoliation of 2D materials, *Advanced Sustainable Systems* 6 (11) (2022) 2200277.
- [31] J. Occhiuzzi, et al., The quest for green solvents for the sustainable production of nanosheets of two-dimensional (2D) materials, a key issue in the roadmap for the ecology transition in the flatland, *Molecules* 28 (3) (2023) 1484.
- [32] L.A. Belyaeva, et al., Hydrophilicity of graphene in water through transparency to polar and dispersive interactions, *Advanced materials* 30 (6) (2018) 1703274.
- [33] M. Buzaglo, et al., Critical parameters in exfoliating graphite into graphene, *Phys. Chem. Chem. Phys.* 15 (12) (2013) 4428–4435.
- [34] L. Huang, et al., Graphene-based conducting inks for direct inkjet printing of flexible conductive patterns and their applications in electric circuits and chemical sensors, *Nano Res.* 4 (2011) 675–684.
- [35] V. Chabot, et al., High yield production and purification of few layer graphene by Gum Arabic assisted physical sonication, *Sci. Rep.* 3 (1) (2013) 1378.
- [36] P. Turner, et al., Controlled sonication as a route to in-situ graphene flake size control, *Sci. Rep.* 9 (1) (2019) 8710.
- [37] S. Barwich, U. Khan, J.N. Coleman, A technique to pretreat graphite which allows the rapid dispersion of defect-free graphene in solvents at high concentration, *J. Phys. Chem. C* 117 (37) (2013) 19212–19218.
- [38] J.-H. Ding, H.-R. Zhao, H.-B. Yu, A water-based green approach to large-scale production of aqueous compatible graphene nanoplatelets, *Sci. Rep.* 8 (1) (2018) 5567.
- [39] R. Patidar, et al., Co-solvent exfoliation of layered titanium diboride into few-layer-thick nanosheets, *Ceram. Int.* 46 (18) (2020) 28324–28331.
- [40] J. Kim, et al., Direct exfoliation and dispersion of two-dimensional materials in pure water via temperature control, *Nat. Commun.* 6 (1) (2015) 8294.
- [41] S. Haar, et al., Enhancing the liquid-phase exfoliation of graphene in organic solvents upon addition of n-octylbenzene, *Sci. Rep.* 5 (1) (2015) 16684.
- [42] E.P. Nguyen, et al., Investigation of two-solvent grinding-assisted liquid phase exfoliation of layered MoS₂, *Chem. Mater.* 27 (1) (2015) 53–59.
- [43] R. Boucher, Sonochemistry at low and high ultrasonic frequencies, *Br. Chem. Eng.* 15 (3) (1970), 363–&.
- [44] M. Tan, et al., Characterisation of improved foam aeration and rheological properties of ultrasonically treated whey protein suspension, *Int. Dairy J.* 43 (2015) 7–14.
- [45] A.V. Tyurmina, et al., Ultrasonic exfoliation of graphene in water: a key parameter study, *Carbon* 168 (2020) 737–747.
- [46] M.U. Arshad, et al., Synthesis of 2D Molybdenum Disulfide (MoS₂) for enhancement of mechanical and electrical properties of polystyrene (PS) polymer, *Polym. Test.* 90 (2020) 106646.
- [47] M. Liang, et al., Improving stability of organometallic-halide perovskite solar cells using exfoliation two-dimensional molybdenum chalcogenides, *npj 2D Materials and Applications* 4 (1) (2020) 40.
- [48] N. Zheng, L. Wang, Z. Sun, The effects of ultrasonication power and time on the dispersion stability of few-layer graphene nanofluids under the constant ultrasonic energy consumption condition, *Ultrason. Sonochem.* 80 (2021) 105816.
- [49] L. Rozenberg, *High-Intensity Ultrasonic Fields*, Springer Science & Business Media, 2013.
- [50] S. Pilli, et al., Ultrasonic pretreatment of sludge: a review, *Ultrason. Sonochem.* 18 (1) (2011) 1–18.
- [51] T. Leighton, *The Acoustic Bubble*, Academic press, 2012.
- [52] I. Tzanakis, et al., Characterisation of the ultrasonic acoustic spectrum and pressure field in aluminium melt with an advanced cavitometer, *J. Mater. Process. Technol.* 229 (2016) 582–586.
- [53] L. Wang, et al., Towards a reference cavitating vessel Part III—design and acoustic pressure characterization of a multi-frequency sonoreactor, *Metrologia* 52 (4) (2015) 575.
- [54] J.H. Bang, K.S. Suslick, Applications of ultrasound to the synthesis of nanostructured materials, *Advanced materials* 22 (10) (2010) 1039–1059.
- [55] S. Brems, et al., Nanoparticle removal with megasonics: a review, *ECS Journal of Solid State Science and Technology* 3 (1) (2013) N3010.
- [56] G.B. Lebon, et al., Ultrasonic liquid metal processing: the essential role of cavitation bubbles in controlling acoustic streaming, *Ultrason. Sonochem.* 55 (2019) 243–255.
- [57] E.M. Joyce, X. Wu, T.J. Mason, Effect of ultrasonic frequency and power on algae suspensions, *Journal of Environmental Science and Health Part A* 45 (7) (2010) 863–866.
- [58] M. Minnaert, XVI. On musical air-bubbles and the sounds of running water, *London, Edinburgh Dublin Phil. Mag. J. Sci.* 16 (104) (1933) 235–248.
- [59] I. Tzanakis, K. Pericleous, D. Eskin, *Experimental and Numerical Investigation of Acoustic Pressures in Different Liquids*, 2018.
- [60] I. Tzanakis, et al., Characterizing the cavitation development and acoustic spectrum in various liquids, *Ultrason. Sonochem.* 34 (2017) 651–662.
- [61] C. Ohl, R. Ikink, Shock-wave-induced jetting of micron-size bubbles, *Phys. Rev. Lett.* 90 (21) (2003) 214502.
- [62] I. Tzanakis, et al., Incubation pit analysis and calculation of the hydrodynamic impact pressure from the implosion of an acoustic cavitation bubble, *Ultrason. Sonochem.* 21 (2) (2014) 866–878.
- [63] M. Sirotyuk, *Experimental investigations of ultrasonic cavitation*, in: *High-Intensity Ultrasonic Fields*, Springer, 1971, pp. 261–343.
- [64] K. Yasuda, H. Matsushima, Y. Asakura, Generation and reduction of bulk nanobubbles by ultrasonic irradiation, *Chem. Eng. Sci.* 195 (2019) 455–461.

- [65] T.-H. Kim, H.-Y. Kim, Disruptive bubble behaviour leading to microstructure damage in an ultrasonic field, *J. Fluid Mech.* 750 (2014) 355–371.
- [66] Q. Zeng, et al., Wall shear stress from jetting cavitation bubbles, *J. Fluid Mech.* 846 (2018) 341–355.
- [67] Y. Wang, et al., Experimental and numerical investigation of cavitation-induced erosion in thermal sprayed single splats, *Ultrason. Sonochem.* 52 (2019) 336–343.
- [68] Z. Shen, et al., Preparation of graphene by jet cavitation, *Nanotechnology* 22 (36) (2011) 365306.
- [69] E.B. Flint, K.S. Suslick, The temperature of cavitation, *Science* 253 (5026) (1991) 1397–1399.
- [70] J.T. Han, et al., Extremely efficient liquid exfoliation and dispersion of layered materials by unusual acoustic cavitation, *Sci. Rep.* 4 (1) (2014) 5133.
- [71] J.A. Morton, et al., New insights into sono-exfoliation mechanisms of graphite: in situ high-speed imaging studies and acoustic measurements, *Mater. Today* 49 (2021) 10–22.
- [72] C. Petrier, et al., Sonochemical degradation of phenol in dilute aqueous solutions: comparison of the reaction rates at 20 and 487 kHz, *The Journal of Physical Chemistry* 98 (41) (1994) 10514–10520.